X-ray rocking curve analysis of superlattices

V. S. Speriosu[a] and T. Vreeland, Jr.
California Institute of Technology, Pasadena, California 91125

(Received 16 March 1984; accepted for publication 7 May 1984)

We present detailed analyses of x-ray double-crystal rocking curve measurements of superlattices. The technique measures depth profiles of structure factor, and profiles of perpendicular and parallel strains relative to the underlying substrate. In addition to providing a detailed picture of the state of stress, the profiles are a direct measure of the composition modulation. The thickness of the period of modulation and the average strain are determined with a precision of $\sim 1\%$. The detailed structure of the period is determined to $\sim 5\%$. We obtain an expression relating the structure of the rocking curve to the structure of the period. This expression allows analytic determination of the structure without Fourier transformation or computer fitting. We show the influence of small random fluctuations in layer thicknesses and strains. The technique is applied to a 15-period GaAlAs/GaAs and a ten-period AlSb/GaSb superlattice grown on ⟨100⟩ GaAs and ⟨100⟩ GaSb substrates, respectively. In the former, the thickness of the period was 676 Å and the perpendicular strain varied between zero for the GaAs layer and 0.249% for the layer with peak (93%) Al concentration. Transition regions, ~ 100 Å thick, with continuously varying composition, were found between the GaAs and the $Ga_{0.07}Al_{0.93}As$ layers. Fluctuations in structural properties were less than 5% of the average. The AlSb/GaSb superlattice had a period of 610 Å with sharp transition regions between the layers and negligible fluctuations from period to period. The perpendicular strains were -0.03% and 1.25%, respectively, for the GaSb and AlSb layers. A uniform parallel strain of 0.03% was found throughout the superlattice. Nonzero parallel strain indicates that a small fraction of the misfit between the superlattice and the substrate is plastically accommodated by net edge dislocations lying in a narrow region (a few hundred Å thick) at the interface with the substrate. The net number of edge dislocations was calculated to be $\sim 1 \times 10^4/cm^2$. The measured perpendicular strains were in excellent agreement with the values calculated from bulk lattice parameters, elastic properties, and the parallel strain. For both superlattices, the standard deviation of random atomic displacements away from perfect crystal sites was below 0.1 Å, in agreement with reported ion channeling and electron diffraction measurements of superlattices. The rocking curve method is a major tool for quantitative analysis of superlattices.

I. INTRODUCTION

Superlattices[1] are a class of epitaxial materials grown by periodic depth modulation of the composition. Recent improvements in growth methods have produced superlattices of nearly perfect crystallinity whose electrical and optical properties can be tailored for various applications. Since the free lattice parameters of the alternating layers are frequently unequal, the modulation of the composition results in a modulated strain. Electrical and optical properties of these devices depend on the state of strain as well as on the composition modulation.[2] The strain in lattice mismatched superlattice layers has been the subject of a series of measurements by ion channeling[3–6] and electron diffraction.[7] Ion channeling has detected periodic changes in crystal channel direction corresponding to distortions of the crystallographic unit cells in the superlattice layers. If a number of nontrivial basic assumptions are made[4–6] concerning the geometry of the distortion, the change in channel direction can be interpreted as a measure of the relative strain in the alternating layers. Electron diffraction has measured absolute distortion in such layers,[7] but with limited precision. Although capable of measuring strain values from 10^{-8} upward, x-ray diffraction has remained relatively unused in the study of superlattices.

Bragg case double-crystal x-ray rocking curves are highly sensitive to strain in epitaxial structures, as shown by their application to semiconductor heterostructures,[8–11] diffusion layers,[12–14] and ion-implanted layers.[15–19] Quantitative analysis[12–14,16] of experimental rocking curves can provide depth profiles of strain with a precision often approaching 2% of quoted values. In general, no assumptions need be made about the geometry of lattice distortion. In epitaxial layers, the scattering of x rays can be modeled[16] to very good approximation by the single-scattering or kinematical theory. The mathematical simplicity of this theory enables rapid computer calculation of rocking curves corresponding to arbitrary structures. By fitting experimental curves, the actual structure can be obtained. The rocking curve method is rapid, nondestructive, requires no sample preparation, and is exceedingly simple.

In an early paper,[20] Segmüller *et al.* gave detailed interpretations of rocking curves of GaAs/AlAs superlattices. Excellent agreement was found between measured intensities and intensities calculated using periodic modulation of strain and structure factor. The modulation was a step function corresponding to the nominal modulation in composi-

[a] Present Address: IBM, San Jose Research Laboratory, San Jose, California 95193.

 0021-8979/84/181591-10$02.40

tion. The strain included a component due to elastic accomodation of the misfit between AlAs and GaAs. More recently, the Fourier transform relationship between the rocking curve on one hand, and the strain and structure factor distributions on the other, was used to measure interdiffusion in annealed GaAs/AlAs superlattices.[21] Due to the small mismatch in lattice parameter between GaAs and AlAs, nonzero strain in directions parallel to the surface was neither expected nor considered in detail in the above references.

In this paper, the diffraction model presented in Ref. 16 is applied to superlattices. Relationships are obtained between the structure of the rocking curve and the structure of the superlattice. These relationships allow direct determination of the structure of the superlattice, without the need to resort to computer fitting or Fourier transformation. In addition to strains in the direction perpendicular to the surface, profiles of parallel strain and structure factor are included in the model. The sensitivity of the rocking curve to the structure of the superlattice period and the effect of random fluctuations from period to period are demonstrated. The method is applied to a GaAlAs/GaAs and an AlSb/GaSb superlattice to obtain depth profiles of perpendicular and parallel strain. Finally, Vegard's law and elasticity theory are used to convert the strain profiles into composition profiles.

II. REFLECTING POWER OF A SUPERLATTICE

It is convenient to define the x-ray strains of an epitaxial film with respect to the substrate, since these are determined directly from the rocking curve. Denoting the film and the substrate by f and s, respectively, for an arbitrary set of planes, there is, in general, a difference $\Delta d = d_f - d_s$ in interplanar d spacing. The difference depends on the particular deformation as well as on the planes. In principle, the strain $\bar{\bar{\epsilon}}$ is a tensor with unequal normal and shear components. For cubic crystals of arbitrary orientation, such as $\langle 311 \rangle$, it is necessary to consider shear strains.[22,8] But for layers grown along the $\langle 100 \rangle$, $\langle 110 \rangle$, or $\langle 111 \rangle$ directions, the principal strains are perpendicular and parallel to the layer. In these directions, the x-ray strains $\epsilon^{\perp}$ and $\epsilon^{\parallel}$ are the fractional differences in interatomic spacing between the film and the substrate. The strains are related to the difference in d spacing through

$$\Delta d/d_s = \epsilon^{\perp} \cos^2 \psi + \epsilon^{\parallel} \sin^2 \psi, \tag{1}$$

where ψ is the angle between the planes and the surface. For perfectly coherent epitaxy, $\epsilon^{\parallel} \equiv 0$ regardless of the mismatch between the free film and the free substrate. Even under partial relaxation ($\epsilon^{\parallel} \neq 0$), this condition imposes stresses of opposite signs in the layer and substrate, and in the simplest case produces tetragonal distortions and bending. Second-order variations of $\epsilon^{\parallel}$ with direction in the plane of the layer occur for nonorthotropic orientations. Since the thickness of the substrate is usually two orders of magnitude greater than the thickness of the layer, the strains in the substrate are usually two orders of magnitude smaller than those in the film. To a good approximation, the substrate is unstrained and one may substitute the free substrate interplanar spacing d_s^0 for d_s in Eq. (1). If the free-lattice parameter of the film is known, it is a simple matter to convert the x-ray strain, defined relative to the substrate, to the strain of elasticity theory, defined relative to the free film. In a later section, we apply elasticity theory to calculate the elastic strains of the superlattice, the substrate elastic strain, and the bending radius of the structure.

For diffraction calculations, a uniform epitaxial layer is described by its thickness t, structure factor F, perpendicular and parallel strains $\epsilon^{\perp}$ and $\epsilon^{\parallel}$, and normal absorption coefficient μ. With respect to the inward normal to the surface, the direction cosines of the incident and diffracted waves are γ_0 and γ_H, respectively. The angle between the diffracting planes and the surface is ψ. Associated with the epitaxial layer and the particular reflection are the quantities A and Y,[23]

$$A = \frac{r_e \lambda |F| t}{V \sqrt{|\gamma_0 \gamma_H|}}, \tag{2}$$

$$Y = -\sqrt{\frac{\gamma_0}{|\gamma_H|}} \frac{\pi V \sin 2\theta_B}{r_e \lambda^2 |F|} (\Delta\omega), \tag{3}$$

where r_e is the classical electron radius, λ is the x-ray wavelength, V is the volume of the unit cell, and θ_B is the Bragg angle of the substrate. The differential angle $\Delta\omega$ is

$$\Delta\omega = \theta - \theta_B + (\epsilon^{\perp} \cos^2 \psi + \epsilon^{\parallel} \sin^2 \psi) \times \tan \theta_B \pm (\epsilon^{\perp} - \epsilon^{\parallel}) \sin \psi \cos \psi, \tag{4}$$

where θ is the grazing angle of incidence with respect to the diffracting planes. The $+$ or $-$ sign is chosen according to whether the angle of incidence with respect to the surface is $\theta_B - \psi$ or $\theta_B + \psi$, respectively. In Eq. (4), the first term involving strains represents a change in d spacing while the second is due to the rotation of the planes. Equation (4) differs in two ways from Eq. (6) in Ref. 16. One is due to the inclusion of parallel strain. In addition, the dependence on ψ in Eq. (4) is valid for any Bragg case $\theta_B + \psi$, whereas Eq. (6) in Ref. 16 is valid only for $\theta_B + \psi \leqslant \pi/2$.[24]

An arbitrary depth profile of strains and structure factor can, for computational convenience and with sufficient accuracy, be represented by a discrete structure of N laminae. The normalized amplitude diffracted by such a structure is[16]

$$E_N = i \sqrt{\frac{\gamma_0}{|\gamma_H|}} \sum_{j=1}^{N} a_j e^{-i(A_j Y_j + \phi_j)} \frac{\sin A_j Y_j}{Y_j}, \tag{5}$$

where

$$a_j = \exp\left(-\mu \frac{\gamma_0 + |\gamma_H|}{2|\gamma_0 \gamma_H|} \sum_{i=j+1}^{N} t_i \right),$$

$$a_N = 1,$$

$$\phi_j = 2 \sum_{i=1}^{j-1} A_i Y_i,$$

$$\phi_1 = 0,$$

and each lamina j has its own A_j and Y_j.

A superlattice is a special case of the arbitrary laminar structure. In its simplest form, the superlattice period consists of two layers, labeled a and b, each with its own thickness, strains, structure factor, and the corresponding A_a, Y_a

and A_b, Y_b. For M superlattice periods and neglecting normal absorption, the diffracted amplitude [Eq. (5)] becomes

$$E_M = i\sqrt{\frac{\gamma_0}{|\gamma_H|}}\, e^{-i\beta} F_s \frac{\sin[M(A_a Y_a + A_b Y_b)]}{\sin(A_a Y_a + A_b Y_b)}, \quad (6)$$

where

$$\beta \equiv (M-1)(A_a Y_a + A_b Y_b) + A_a Y_a$$

and

$$F_s \equiv \frac{\sin A_a Y_a}{Y_a} + e^{-i(A_a Y_a + A_b Y_b)} \frac{\sin A_b Y_b}{Y_b}. \quad (7)$$

The quantity F_s can be regarded as the structure factor of one superlattice period. The sinusoidal term in the numerator of Eq. (6) produces zeros with a period $\Delta\theta_M$ given by

$$M\Delta(A_a Y_a + A_b Y_b) = \pi$$

or

$$\Delta\theta_M = \frac{\lambda|\gamma_H|}{M(t_a + t_b)\sin 2\theta_B} \quad (8)$$

from which the total thickness $M(t_a + t_b)$ of the superlattice can be determined. However, for typical samples (~ 1 μm thick) lateral nonuniformities frequently result in a convolution of the rapid oscillations. The more slowly varying sinusoidal term in the denominator of Eq. (6) produces observable peaks at

$$A_a Y_a + A_b Y_b = n\pi; \quad (9)$$

hence, the peaks are labeled 0, ± 1, ± 2, etc. The spacing $\Delta\theta_P$ between the peaks yields the superlattice periodicity p,

$$p \equiv t_a + t_b = \frac{\lambda|\gamma_H|}{\Delta\theta_P \sin 2\theta_B}. \quad (10)$$

The superlattice zeroth-order peak is located at an angle $\Delta\theta_0$ from the substrate peak. From Eq. (9),

$$\begin{aligned} -\Delta\theta_0 &= k_1\langle\epsilon^{\perp}\rangle + k_2\langle\epsilon^{\parallel}\rangle, \\ k_1 &= \cos^2\psi \tan\theta_B \pm \sin\psi\cos\psi, \\ k_2 &= \sin^2\psi \tan\theta_B \mp \sin\psi\cos\psi, \end{aligned} \quad (11)$$

where $\langle\ \rangle$ denotes depth averaging (over the superlattice period) and the sign is chosen as described above. The amplitude of the nth-order peak is proportional to the superlattice structure factor [Eq. (7)] evaluated at angles determined by Eq. (9). Using n as a subscript,

$$\begin{aligned} F_{sn} &= \sin A_a Y_{an}\left(\frac{1}{Y_{an}} - \frac{1}{Y_{bn}}\right) \\ &= \frac{\sin A_a Y_{an}}{A_a Y_{an}}\left(A_a + \frac{A_b}{1 - (n\pi/A_a Y_{an})}\right). \end{aligned} \quad (12)$$

Since Y_{an} is related to Y_{a0} through Eqs. (10) and (3), Eq. (12) depends on A_a, A_b, and Y_{a0} only. For $n = 0$, this reduces to

$$F_{s0} = \frac{\sin A_a Y_{a0}}{A_a Y_{a0}}(A_a + A_b) \approx (A_a + A_b), \quad A_a Y_{a0} \ll 1. \quad (13)$$

Thus, the amplitude of the zeroth-order peak measures $F_a t_a + F_b t_b$, where F_a and F_b are the crystallographic structure factors of layers a and b, respectively. The approximation in Eq. (13) is quite good for typical strong reflections and products of strain modulation and period thickness below $\sim 1\% \times 300$ Å. In these cases, the zeroth-order peak is more intense than higher-order peaks. For larger strains and thicknesses, the approximation in Eq. (13) breaks down and the zeroth-order peak may be less intense than higher-order peaks. In a later section, we give examples of both regimes.

From Eq. (6), it is clear that the basic structure of the rocking curve is determined by the structure of the superlattice period. The number of peaks, their locations, and relative amplitudes are independent of the number of periods, provided this number is greater than 1. For M periods and negligible absorption, the overall intensity of the rocking curve goes as M^2. A perfect superlattice is described by six parameters: t_a, t_b, $\bar{\bar{\epsilon}}_a$, $\bar{\bar{\epsilon}}_b$, F_b/F_a, and M. To determine these parameters, one can use Eqs. (8), (10), (11), and (13), and Eq. (12) evaluated for the ± 1 peaks. The locations and amplitudes of peaks corresponding to $|n| > 1$ are completely determined by the six parameters. To separate the components of $\bar{\bar{\epsilon}}_a$ and $\bar{\bar{\epsilon}}_b$, one needs at least two rocking curve measurements. The availability of a large number of intense reflections with varying degrees of asymmetry enables the verification of the internal consistency of the depth profiles of strain and structure factor. In fact, the present method can be extended to arbitrary deformations, including shear strains. For each additional strain component, an additional rocking curve measurement is needed.

The solution of the six simultaneous equations is straightforward provided the condition in Eq. (13) is satisfied. Since this is not always the case, it may be necessary to consider higher-order peaks. Alternatively, since the condition of Eq. (13) depends on the Bragg angle and on ψ as well as on the strain and thickness, it is almost always possible to use a reflection where the zeroth-order peak is the most intense. In practice, the number of periods and the approximate composition modulation are known from the growth conditions. One can calculate *a priori* F_a and F_b from the nominal composition. This reduces the number of unknowns to four without changing the number of equations (six). Thus, for a perfect or nearly perfect superlattice, we are able to determine its structure by following a specified algorithm and are not dependent on computer fitting.

If the structure of the superlattice period has more detail than the bilayer model assumed above, it is nevertheless clear that the form of Eq. (6) remains valid. By straightforward extension, Eqs. (6) and (7) can describe diffraction in superlattices with an arbitrary number of sublayers in one period. For each additional sublayer, the intensity of an additional high-order peak must be considered. However, Eqs. (10) and (11), which determine the periodicity and the average strain, remain applicable regardless of the structure of the period.

Real superlattices are imperfect. The strain and thickness values fluctuate from period to period. One result of this is that the periodicity determined from Eq. (6) is noncommensurate with crystallographic unit cells. If the number of periods is small and the fluctuations are arbitrarily large, the rocking curve rapidly loses the structure predicted by Eq. (6). In such cases, one can return to Eq. (5), which is valid for arbitrary depth profiles in thin layers, and match the experi-

mental rocking curve with the aid of a computer. Although convergence to a good fit cannot be guaranteed, the sensitivity of the rocking curve to the strain profile ensures that a good fit can only be obtained with the "true" profile.[16,19] The importance of obtaining a good fit (examples may be found in Refs. 10–14, 16, and 19) cannot be overemphasized.

For small fluctuations and a large number of periods, one can describe the frequency of the particular fluctuation by a probability ρ. If the thickness of layer a varies, corresponding to a variation ΔA in A_a, and the probability of ΔA is Gaussian with standard deviation U_A, it is straightforward to show that the average structure factor $\langle F_{sn} \rangle$ is given by

$$\langle F_{sn} \rangle = \exp(-2Y_{an}^2 U_A^2) F_{sn}^0, \tag{14}$$

where F_{sn}^0 corresponds to no fluctuation. The exponential term is analogous to a Debye–Waller factor. Since $|Y_{an}|$ increases with n, high-order peaks are diminished much more than low-order peaks. The intensity lost at each peak will, of course, be seen in the rise of the background intensity between the peaks. From symmetry, a fluctuation in A_b produces a similar result. If both A_a and A_b fluctuate, the structure factors of high-order peaks diminish even more rapidly. The influence of strain fluctuations is less transparent, but we shall show by example that it also decreases the intensity of high-order peaks.

From a practical point of view, the existence of transition regions in the superlattice period and the possibility of fluctuations from period to period are of great interest. To explore these possibilities in real samples, we adopt an approach combining analytic determination with trial-and-error fitting. The locations and intensities of the three low-order peaks yield the structure of the superlattice assuming a bilayer distribution in each period and perfect periodicity. These values of strains, structure factors, and thicknesses provide an initial distribution for a calculated rocking curve. Discrepancies between measured and calculated intensities of high-order peaks are then minimized by trial-and-error fitting. The structure of the experimental curve will suggest whether the discrepancies are due to fluctuations from period to period, to transition regions in each period, or both.

The frequent presence[4,7,25] of a buffer layer grown between the superlattice and the substrate also necessitates a departure from analytic structure determination. For a buffer of arbitrary composition modulation, it is not possible to derive simple relationships between the rocking curve and the superlattice-cum-buffer structure. If the buffer is uniform, as is often the case, it will contribute an additional peak to the rocking curve. The location and intensity of this peak yield the strain and thickness of the buffer.[25]

For calculations of rocking curves, as in Ref. 16, the reflecting power of the epitaxial structure is added to that of the substrate, adjusted for normal absorption in the epitaxial structure. The substrate reflecting power is obtained using only the σ component of the dynamical theory[23] result for thick, nonabsorbing, perfect crystals. For computational speed we neglect the substrate π component, which is always narrower than the σ component. For the same reason we do not interfere the amplitude of the epitaxial structure with that of the substrate. These omissions do not produce observable errors since the plane-wave solutions are always convolved with Gaussians whose widths are greater than the Darwin width.[23]

III. EXPERIMENT

Superlattice samples were provided to us by external sources. The $Ga_xAl_{1-x}As/GaAs$, $x \simeq 0.1$, sample was grown[26] by metalorganic chemical vapor deposition (MOCVD) on a ⟨100⟩ GaAs substrate. The nominal number of layers and layer thinckness were 30 and 200 Å, respectively (15 periods, 400 Å per period). The AlSb/GaSb sample was grown[27] by molecular beam epitaxy (MBE) on a ⟨100⟩ GaSb substrate. The nominal number of layers and layer thickness were 20 and 300 Å, respectively (10 periods, 600 Å per period). For both kinds of superlattices, the substrates were found to be oriented $\sim 2°$ off the ⟨100⟩ axis. The actual misorientation was taken into account for the values of ψ, γ_0, and γ_H.

Double-crystal x-ray rocking curves were obtained using the Fe $K_{\alpha 1}$ (200), (400), and (422) reflections and the Cu $K_{\alpha 1}$ (422) reflection. With the exception of the (200) reflection, the Bragg angle is near 45° and the σ component is dominant.[23] The symmetric (200) and (400) reflections are sensitive to $\epsilon^{\perp}$ only, while the asymmetric (422) reflections measure both $\epsilon^{\perp}$ and $\epsilon^{\parallel}$ [see Eq. (4) above]. Depending on asymmetry and Bragg angle the sensitivity to $\epsilon^{\parallel}$ is either lower or greater than that to $\epsilon^{\perp}$. The use of more than one reflection permits verification of the internal consistency of the strain profiles. The x-ray beam was first collimated and rendered nearly monochromatic by (400) reflection in ⟨100⟩ Si or GaAs for the Fe $K_{\alpha 1}$ (200), (400), and (422) reflections and by (333) reflection in ⟨111⟩ Si for the Cu $K_{\alpha 1}$ (422) reflections. With the exception of the (200) reflection, the Bragg angles of the first crystal and the sample are nearly equal and the rocking curve is insensitive to the finite width of the $K_{\alpha 1}$ line. Even for the (200) reflection, with the $K_{\alpha 2}$ line blocked by the slits, the broadening due to the use of dispersive setting did not significantly affect the measured curve. In all cases, the divergence of the beam incident on the sample was less than 20 arcsec. Except for the (422), $\gamma_0 < |\gamma_H|$ reflection, the spot size at the sample was limited by a set of slits to 0.5×1 mm or less. For the (422), $\gamma_0 < |\gamma_H|$ reflection, due to the low grazing angle of incidence, the spot size was greater than the size of the sample, vitiating absolute measurement of reflecting power. The incident beam intensity was 10^4–10^5 counts/sec, depending on the reflection and spot size. Rocking curves were obtained using a microprocessor-controlled diffractometer with a step-scan resolution of 10^{-4} deg.

IV. RESULTS AND DISCUSSION

The two kinds of superlattices discussed below are examples of extreme cases of strain variation likely to be found in practice. For the GaAlAs/GaAs superlattice, the maximum strain is below 0.3%, while for the AlSb/GaSb superlattice, the strain modulation is greater than 1%. In both cases, the nominal thickness of the period is large (400–600 Å) so that for the AlSb/GaSb superlattice the condition in Eq. (13) above is not satisfied, i.e., the zeroth-order peak is

less intense than higher-order peaks. For the GaAlAs/GaAs superlattice, the zeroth-order peak is the most intense. The calculated curves were obtained using Eq. (11) in Ref. 16 with structure factors based on nominal composition and tabulated atomic scattering factors[28] (see Table I). Normal absorption coefficients were averaged over the superlattice period.

A. GaAlAs/GaAs superlattice

Figure 1(a) shows measured (dashed line) and calculated (solid line) Fe $K_{\alpha 1}$ (400) rocking curves of the GaAlAs/GaAs superlattice. In the experimental curve, in addition to the substrate peak (located at zero), seven superlattice peaks are clearly visible. These are obviously not the rapid oscillations of Eq. (8), but peaks given by Eq. (9) above. Their spacing yields an average superlattice period thickness $p = 676 \pm 2$ Å. The location $\Delta\theta_0 = -0.0641°$ of the zeroth-order peak yields, through Eq. (11), $\langle\epsilon^{\perp}\rangle = 0.118\%$. The (400) rocking curve gives no information on $\epsilon^{\parallel}$, but previous work has shown[8,29,30] that it is zero for epitaxial AlAs layers, up to several microns thick, grown on GaAs.

Assuming that the nominal GaAs layer is indeed GaAs, its perpendicular (and parallel) strain must be zero. The task of determining the strain profile in the superlattice period is thus reduced to determining the thickness and strain of the GaAlAs layer. Using the ratio of the amplitude of the $+1$ peak to that of the zeroth peak and the appropriate structure factors from Table I, Eq. (12) yields a thickness and strain of 320 Å and 0.249%, respectively, for the GaAlAs layer. The same values are obtained using the ratio of the amplitude of the -1 peak to that of the zeroth peak. The agreement between these two determinations shows that the initial assumption of zero strain in the GaAs layer is valid. Had this assumption been false, the $+1$ and -1 peaks would have yielded different thicknesses and strains for the GaAlAs layer. The calculated rocking curve of Fig. 1(a) was obtained from this initial strain and structure factor distribution. The calculated curve reproduces very well the locations of the observed peaks as well as the intensities of the three low-order peaks. The slight discrepancy in the intensities of the $+1$ and -1 peaks is due to the small error in thickness and strain obtained from Eq. (12) which neglected absorption, whereas the calculated curve in the figure includes normal absorption. For high-order peaks, the calculated curve generally predicts more intensity than is observed. Since random fluctuations in layer thickness were shown to decrease high-order more than low-order peaks, one may suppose that the discrepancy is due to such fluctuations. Figure 1(b) reproduces the experimental curve of Fig. 1(a) and shows a calculated curve corresponding to random fluctuations of about 5% in layer thicknesses. The agreement with the measured curve is better although certain discrepanices persist. In Fig. 1(c), the calculated curve includes 5% fluctuations in both layer thicknesses and strain values. This results in a further diminution of high-order peaks, but does not elminate all discrepancies. Larger fluctuations would only decrease the quality of the fit. In fact, careful examination of Fig. 1(a) shows that the discrepancy is due to the existence of transition regions in the superlattice period, rather than to fluctuations from period to period. This is best seen for the intensities of the $+3$ and $+4$ peaks (located at $\Delta\theta \simeq 0.25°$ and $\Delta\theta \simeq 0.4°$, respectively). The calculated curve matches the $+4$ peak reasonably well, but overestimates the intensity of the $+3$ peak. Clearly random fluctuations decrease the intensity of the $+4$ peak more than that of the $+3$ peak [Figs. 1(b) and 1(c)]. A much better overall fit, shown in Fig. 1(d), is obtained using the four-layer period of Table II. These values were accepted as sufficiently accurate after a trial-and-error procedure involving about ten iterations. The strain distribution and the structure factor distribution indicate the self-consistent result that the Al concentration varies continuously between the nominal GaAlAs and GaAs layers. Before discussing this result in more detail, we turn to the Fe $K_{\alpha 1}$ (200) rocking curve of the same sample.

Figure 2(a) shows the measured (dashed line) and a calculated (solid line) Fe $K_{\alpha 1}$ (200) rocking curve. Ten superlattice peaks are evident in the experimental curve. Since the Bragg angle for the (200) reflection is only 20.04°, the zeroth-order peak is not well separated from the substrate peak [see Eq. (4) above]. Because in this case the structure factor for GaAs is only 6.64, the substrate peak is very weak and appears as a shoulder on the superlattice zeroth peak. In addition, the low structure factor of the GaAs layers means that effectively only the GaAlAs layers are diffracting. For this reflection, the superlattice acts as if only the GaAlAs layers, separated by nondiffracting material, were present. Thus the rocking curve is very sensitive to the details of the GaAlAs portion of the period, and is less sensitive to the GaAs portion. The calculated curve corresponds to the same strain profile as was used in Fig. 1(a). As before, the step-function distribution gives a reasonably good fit to the experimental curve. The discrepancies are reduced if the four-layer period of Table II is used in the calculation, as shown in Fig. 2(b). Further improvement in the quality of the fit can only be obtained by introducing even finer detail in the structure of the period.

Despite the difference in their structure, the Fe $K_{\alpha 1}$ (400) and (200) rocking curves yield the same structure for the superlattice period. The thickness of the period and the average strain are determined to a precision of $\sim 1\%$. Consideration of only the three lowest-order peaks determines the amplitude of the strain modulation and the relative thickness of the layers to $\sim 15\%$. If a good fit is obtained for high-order peaks, as in Figs. 1(d) and 2(b), the structure of the period, including transition regions, is determined to a precision of $\sim 5\%$.

The thickness of the period (676 Å) is very different from the nominal thickness (400 Å). Since the growth rate

TABLE I. Absolute values of structure factors.

Reflection		GaAs	$Al_{0.9}Ga_{0.1}As$	GaSb	AlSb
Fe K_α	(400)	157.9	116.9	214.2	166.9
	(200)	6.64	61.05	72.4	131.1
	(422)	...	...	191.2	150.1
Cu K_α	(422)	...	...	191.3	151.6

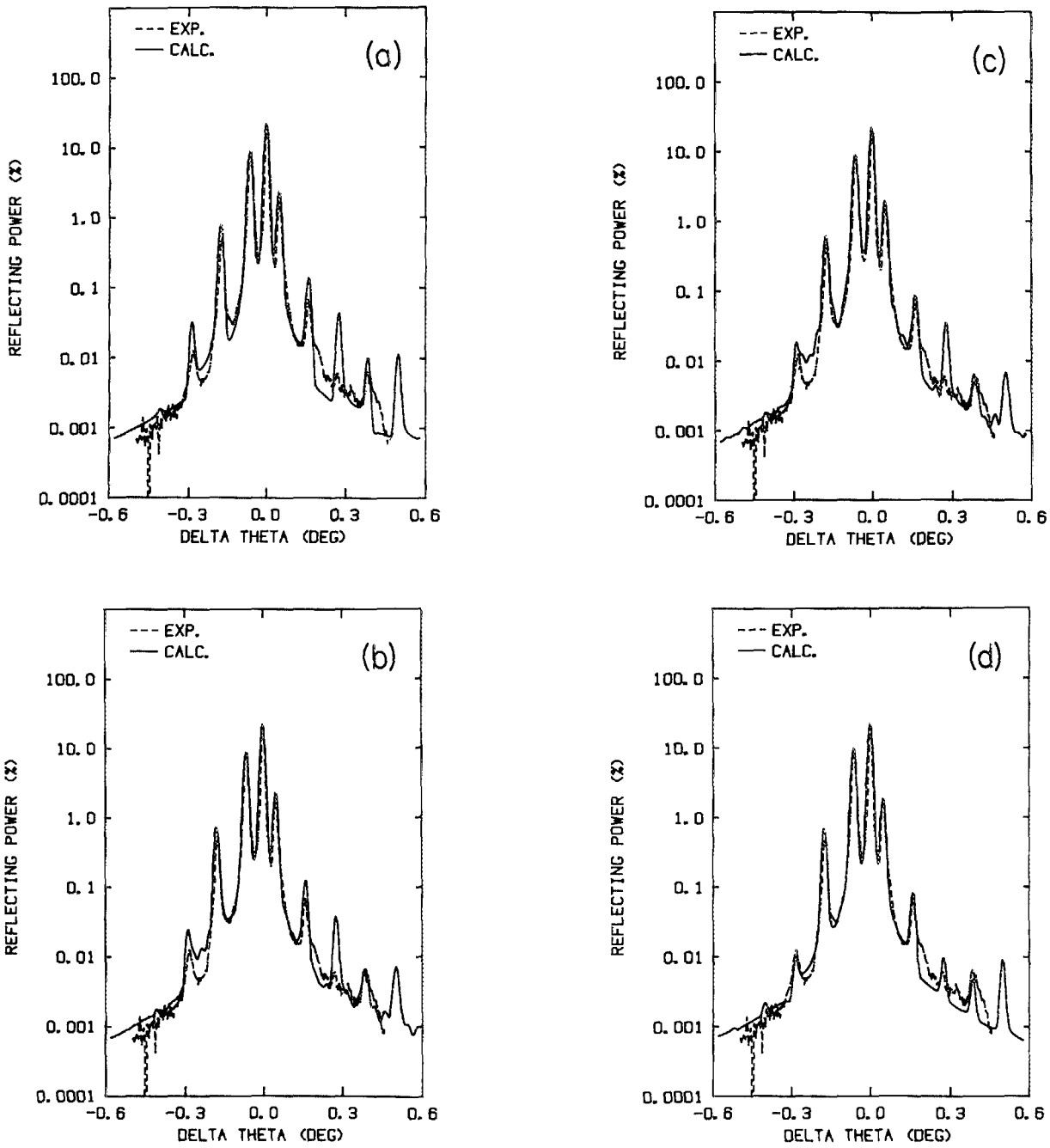

FIG. 1. (a) Measured (dashed line) and calculated (solid line) Fe $K_{\alpha 1}$ (400) rocking curves of GaAlAs/GaAs superlattice. The calculated curve corresponds to the bilayer structure of the period discussed in the text. (b) Fe $K_{\alpha 1}$ (400) rocking curves of GaAlAs/GaAs superlattice. The calculated curve corresponds to ~5% fluctuations in layer thicknesses. (c) Fe $K_{\alpha 1}$ (400) rocking curves of GaAlAs/GaAs superlattice. The calculated curve corresponds to ~5% fluctuations in both layer thicknesses and strains. (d) Fe $K_{\alpha 1}$ (400) rocking curves of GaAlAs/GaAs superlattice. Best fit of experimental curve using the four-layer period of Table II.

during MOCVD is determined by the availability of Ga, an error in its concentration will result in an error in estimated layer thickness. The present reactor was calibrated[26] for much thicker (2000 Å) layers where the finite rise time of the system was short compared to the total growth duration. The effects of finite rise time are also evident in the ~150 Å (Table II) transition regions between the uniform GaAlAs ($\epsilon^{\perp} = 0.249\%$) and GaAs ($\epsilon^{\perp} = 0.00\%$) layers.

B. AlSb/GaSb superlattice

Figure 3 shows experimental and calculated Fe $K_{\alpha 1}$ (400) rocking curves. In addition to the substrate peak, the measured curve contains 14 clearly visible superlattice peaks. As mentioned earlier, due to the combination of large strain modulation and large thickness of the period, the zeroth-order peak is less intense than higher-order peaks. This situation presents the practical problem of identifying the

TABLE II. Strain and Structure factor distributions in the average period of the GaAlAs/GaAs superlattice. Strain is defined relative to the substrate [see Eq. (1)].

Layer	Thickness (Å)	$\epsilon^{\perp}$ (%)	$\lvert F_{400}\rvert$	$\lvert F_{200}\rvert$
a	150	0.180	128.3	46.0
b	170	0.249	116.9	61.05
c	100	0.103	136.5	35.1
d	256	0.000	157.9	6.64

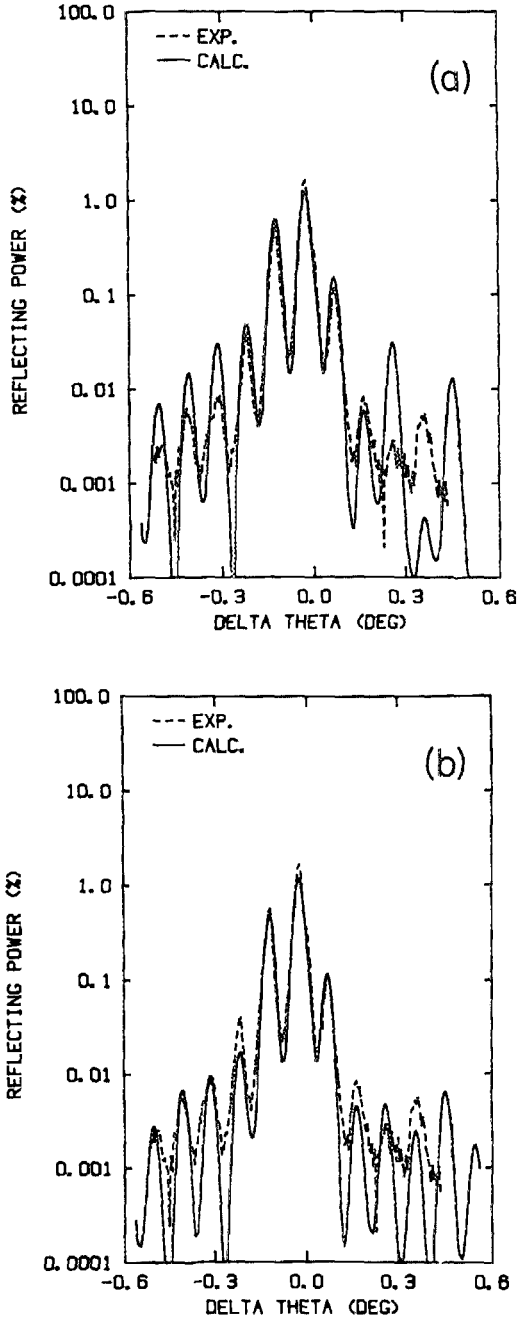

FIG. 2. (a) Fe $K_{\alpha 1}$ (200) rocking curves of GaAlAs/GaAs superlattice. The calculation corresponds to the bilayer period used in Fig. 1(a). (b) Fe $K_{\alpha 1}$ (200) rocking curves of GaAlAs/GaAs superlattice. Best fit using the four-layer period of Table II.

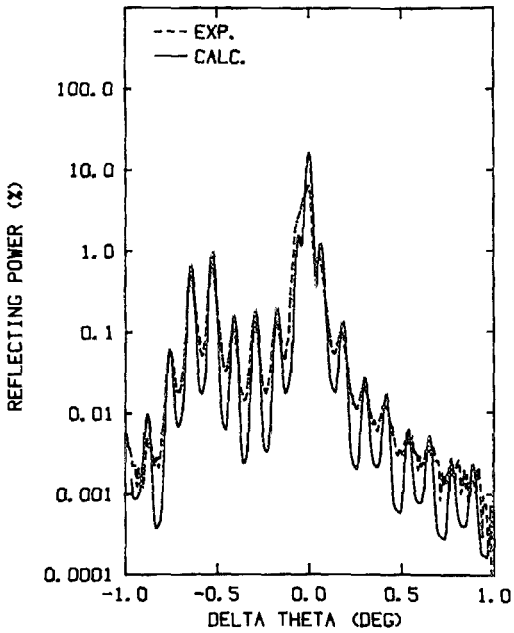

FIG. 3. Fe $K_{\alpha 1}$ (400) rocking curves of AlSb/GaSb superlattice. The calculated curve is based on the bilayer period of Table III.

zeroth-order peak. The simplest way to resolve the dilemma is to calculate a rocking curve using data based on the nominal composition modulation .The actual thickness of the period, 610 ± 2 Å, is determined directly from the measured curve. Using the appropriate structure factors from Table I, the nominal thickness ratio of 1 : 1 in the bilayer model of the period, and assuming zero perpendicular strain in the GaSb layer, one can calculate rocking curves corresponding to various values of perpendicular strain in the AlSb layer. Comparison with the experimental curve immediately shows that the strain in the AlSb layer is around 1.2% while the strain in the GaSb layer is indeed close to zero. Consequently, the zeroth-order peak is at $\Delta\theta_0 \approx -0.29°$ in Fig. 3. This result may be verified by comparing calculated and measured intensities of all peaks. The good agreement shown in Fig. 3 was obtained by trial-and-error adjustment in the structure of the period. For this sample, the structure is very nearly a step function (see Table III). The thickness of the transition region between the two layers is at most 5% of the thickness (305 Å) of the layers. The perpendicular strains are $(1.25 \pm 0.02)\%$ and $(-0.03 \pm 0.02)\%$ for the AlSb and GaSb layers, respectively. Negative perpendicular strain in the GaSb layer implies positive parallel strain, as we show below.

TABLE III. Strain distributions in the average period of the AlSb/GaSb superlattice. Strain is defined relative to the substrate [see Eq. (1)].

Layer	Thickness (Å)	$\epsilon^{\perp}$ (%)	$\epsilon^{\parallel}$ (%)
a	305	1.25	0.03
b	305	−0.03	0.03

The Fe $K_{\alpha 1}$ (200) rocking curves of Fig. 4 yield slightly different values for the period thickness (625 Å) and the strain of the AlSb layer (1.23%). Even though for this reflection $\theta_B = 18.5°$, the condition of Eq. (13) is still not satisfied and the zeroth peak, at $\Delta\theta_0 \approx -0.1°$, is less intense than higher-order peaks. The agreement between the shapes of calculated and measured curves is very good, but the calculated curve is everywhere about a factor of 2 more intense than the measured curve. The discrepancy is not accounted for, but suggests an error in the calculated structure factors or in the measurement of the incident beam intensity, or both.

The Fe $K_{\alpha 1}$ (422), $\gamma_0 > |\gamma_H|$ rocking curves are shown in Fig. 5. Note the much narrower intrinsic width of these curves compared to those of Figs. 3 and 4. The thickness of the period deduced from Fig. 5 is the same as the value obtained with the (400) reflection. For Fe $K_{\alpha 1}$ (422), with $\gamma_0 > |\gamma_H|$, Eq. (4) shows that the sensitivity to parallel strain is ~ 3.5 times greater than that to perpendicular strain. Using the values of $\epsilon^{\perp}$ obtained with (400) and/or (200), the (422) curve yields $\epsilon^{\parallel} = (0.03 \pm 0.02)\%$ for both layers of the period (see Table III).

The sense of asymmetry is reversed for the Cu $K_{\alpha 1}$ (422), $\gamma_0 < |\gamma_H|$ reflection of Fig. 6. In this case, the sensitivity to $\epsilon^{\perp}$ is much greater than that to $\epsilon^{\parallel}$. As mentioned above, for this reflection the angle of incidence with respect to the sample is only $\sim 2°$ and the x-ray spot size was greater than the size of the sample. Thus, the experimental reflecting power was easily underestimated. Nevertheless, the measured and calculated curves have the same shape, confirming the strain profiles obtained with the other reflections. Thus, all four rocking curves (Figs. 3–6), measured at different Bragg angles, with different asymmetries and different wavelengths, correspond to the same structure of the period (Table III).

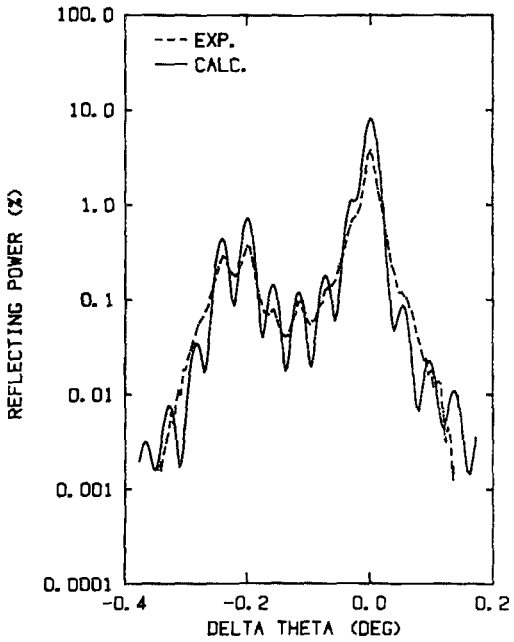

FIG. 5. Fe $K_{\alpha 1}$ (422), $\gamma_0 > |\gamma_H|$ rocking curves of AlSb/GaSb superlattice. The calculated curve used the period of Table III.

The presence of nonzero parallel strain implies the breakdown of perfect coherency between the epitaxial structure and the substrate. In the direction perpendicular to the surface, for $\epsilon^{\parallel} = 0.03\%$ there are three fewer atomic planes in the superlattice for every 10^4 planes in the substrate. Since $\epsilon^{\parallel}$ is uniform throughout the superlattice layers, the partial crystallographic decoupling occurs in a narrow (a few hundred Å thick) region at the interface between the superlattice and the substrate. A parallel strain of 0.03% corresponds to a net number of $\sim 1 \times 10^4\ \alpha/2\ \langle 011 \rangle$ edge dislocations.

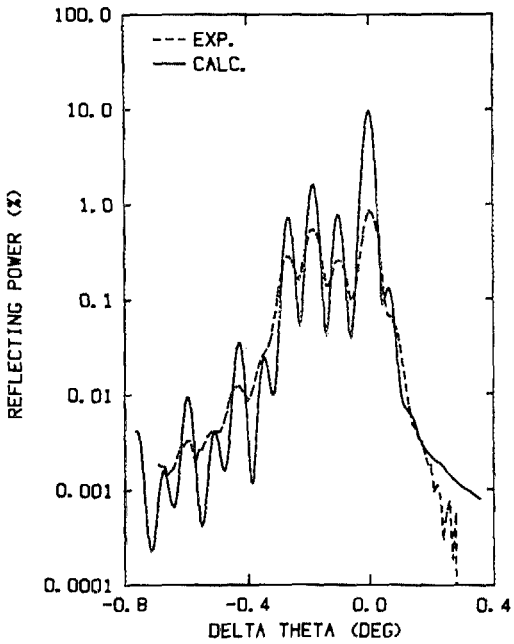

FIG. 4. Fe $K_{\alpha 1}$ (200) rocking curves of AlSb/GaSb superlattice. The calculated curve used the period of Table III.

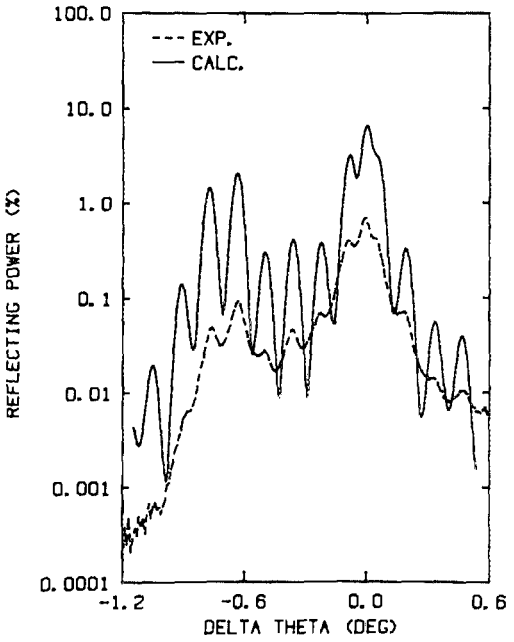

FIG. 6. Cu $K_{\alpha 1}$ (422), $\gamma_0 < |\gamma_H|$ rocking curves of AlSb/GaSb superlattice. The calculated curve used the period of Table III. The absolute reflecting power of the measured curve is underestimated, as discussed in the text.

tions/cm^2 localized in a narrow region at the interface with the substrate. A much larger parallel strain (0.19%) was measured[25] in a $GaAs_xP_{1-x}$/GaP, $x = 0.14$, superlattice grown on a 1-μm $GaAs_yP_{1-y}$, $y = 0.061$, buffer on ⟨100⟩ GaP. The buffer plays a major role in decoupling the superlattice from the substrate.

C. Point defects and lateral inhomogeneities

In addition to providing depth profiles of strain, experimental rocking curves contain information about point defects and lateral inhomogeneities.[16–19] A measure of point defects is obtained from comparison of experimental intensity with that predicted using perfect-crystal structure factors. Point defects lead to a decrease in the magnitude of the structure factor. If point defects are described by a probability distribution of incoherent atomic displacements away from perfect-crystal sites, the standard deviation U of the distribution is readily obtained from the measured curve.[16,19] For the present samples, structure factors were calculated assuming no point defects other than those due to random interchange of Ga and Al corresponding to the local composition. The good agreement between measured and calculated curves obtained above indicates that for both samples the standard deviation U is less than 0.1 Å. This is consistent with the general result obtained by channeling[3–6] and electron diffraction[7] on a variety of superlattices.

Lateral inhomogeneities in composition and extended defects such as dislocations produce lateral variations in strain and undulations in atomic planes. A measure of this undulation is the width of the function used to convolve the plane-wave, planar structure rocking curve. As mentioned earlier, the divergence of the beam incident on the sample was in all cases below 20 arcsec. An increase over this value in the width of the convolving function indicates lateral inhomogeneity in the sample. The calculated curves shown above were convolved with Gaussians of 30–75 arcsec standard deviations. Thus, for both samples, there are undulations of ~ 1 arcmin in atomic planes.

D. Elastic strains and determination of composition

The problem of the distribution of elastic strains in the epitaxial layer and substrate is similar to the bimetal strip problem whose solution may be found in standard texts.[31] The final state of strain may be thought of as resulting from a three-step process: (1) the epitaxial layer is strained to match the in-plane interatomic spacing of a rigid substrate; (2) under the action of the epitaxial layer the nonrigid substrate and layer are strained without bending by an amount yielding zero net force on the structure, but nonzero bending moment; (3) the structure acquires curvature when the bending moment is removed. For imperfectly coherent epitaxy (i.e., the x-ray $\epsilon^{\parallel} \neq 0$), the structure relaxes as if the initial misfit were decreased by the x-ray parallel strain. From Vegard's law for alloyed materials, the (free) lattice parameter varies linearly with composition. Assuming that elastic properties[22] also vary linearly with composition, one can calculate elastic strains for arbitrary combinations of epitaxial layer and substrate. Comparison of calculated and measured strains allows determination of the composition.

Using the commonly accepted[8,20,30] misfit of 1.4×10^{-3} between AlAs and GaAs, and the x-ray strain of layer b in Table II, we obtain a peak Al concentration $x = 0.935$. In layers a and c, the concentration of Al scales with the strain. For the 500-μm-thick GaAs substrate, the radius of curvature is calculated to be -25.5 m. At the interface with the superlattice, the elastic perpendicular and parallel strains of the substrate are -0.001 and $+0.001$%, respectively.

Using lattice parameter values[32] of 6.095 and 6.135 Å for GaSb and AlSb, respectively, and the measured x-ray $\epsilon^{\parallel} = 0.03$%, we calculate x-ray perpendicular strains of -0.027 and 1.27% for the GaSb and AlSb layers, respectively. The agreement with measured values, Table III, is very good. At the interface with the superlattice, the substrate perpendicular and parallel elastic strains are -0.004 and 0.004%, respectively. For the 500-μm-thick substrate, the calculated bending radius is -7.5 m.

For both superlattice samples, the deformation of the substrate is only a few percent of that of the epitaxial structure. This validates the (general) use of the free substrate lattice parameter in the comparison of x-ray and elastic strains in epitaxial structures on thick substrates.

V. CONCLUSION

We have given a simple expression relating the structure of the superlattice period to the structure of the rocking curve. The form of this expression shows at a glance the existence of equally spaced peaks whose intensities are determined by the structure of the superlattice period. The location and intensity of the zeroth (and frequently largest) peak measure the depth-averaged properties of the superlattice. For a perfectly periodic superlattice whose period is a step function, consideration of the three lowest-order peaks provides an analytic determination of the period. For more complicated structures, including transition regions between the layers of the period, one must consider the intensities of higher-order peaks. Small, random fluctuations in layer thicknesses and strains decrease the intensities of high-order peaks with relatively small changes for low-order peaks. The treatment above includes depth profiles of structure factor and perpendicular and parallel strains. Extension to arbitrary deformations, including shear strains, is straightforward. For each additional strain component, an additional rocking curve measurement is needed. The availability of a large number of intense reflections allows verification of the internal consistency of the profiles. The strain profiles, referred to the unit cell of the underlying substrate, are absolute.

We have analyzed a GaAlAs/GaAs and an AlSb/GaSb superlattice. The former is an example of small modulation of strain (GaAlAs on GaAs is frequently called "unstrained") while in the latter the amplitude of strain modulation is 1.28%. Combination of large perpendicular strain and total thickness (6100 Å) in the AlSb/GaSb superlattice produced a departure from perfectly coherent epitaxy. In this sample, a uniform parallel (in-plane) strain of 0.03% was measured. The parallel strain is accomodated by misfit dislocations ($\sim 1 \times 10^4$/cm^2) localized in a narrow region at the interface with the substrate. The measured perpendicular

strain was in excellent agreement with the value calculated from bulk lattice parameters, elastic constants, and the measured parallel strain. In the GaAlAs/GaAs superlattice, the Al content was determined from Vegard's law and elasticity theory.

For the samples studied above, the periodicity and average strain were measured with a precision of $\sim 1\%$. The relative thickness of the layers and the strain modulation are known to $\sim 5\%$. Since for both samples the thickness of the period was large (~ 600 Å), one may ask whether the high precision obtained above will hold for samples with periodicities of 100 Å or less. We believe that this will remain true, because of the availability of a large number of asymmetric reflections. In the generalized A and Y coordinates used above, the structure (i.e., number, spacing, and relative intensities of peaks) of the rocking curve is invariant. One may choose the particular reflection by considering sensitivity and convenience.

The x-ray rocking curve method enjoys a number of advantages over ion channeling, Rutherford backscattering, electron diffraction, and Auger electron spectroscopy, all of which have been used to measure properties of superlattices. The complexity and cost of the apparatus are an order of magnitude lower. The measurement of rocking curves is simple, rapid, and reproducible. The measurement does not destroy the sample. In epitaxial layers, the precision of composition determination is at least as good as that obtained by other techniques. For measurement of strain profiles, the rocking curve is unmatched by either channeling or electron diffraction.

ACKNOWLEDGMENTS

Dr. Bruce M. Paine contributed in a major way to the setting up of our diffractometer and data acquisition and analysis system. During the initial critical stages of the development, Dr. Paine guided us successfully through a morass of hardware and software problems. Since then we have relied on him for general troubleshooting and advice on programming. We are grateful to John Melvin for supplying us with an initial graphics package and to Frank Cosso and Prakash Kasiraj for systems programs. Professor M-A. Nicolet encouraged us at every step of this study. The work was supported by the Defense Advanced Research Projects Agency (S. Roosild) under Contract (MDA 903-82-C-0348).

[1]L. Esaki and L. L. Chang, Phys. Rev. Lett. **33**, 495 (1974).
[2]G. C. Osbourn, J. Appl. Phys. **53**, 1586 (1982).
[3]F. W. Saris, W. K. Chu, C. A. Chang, R. Ludeke, and L. Esaki, Appl. Phys. Lett. **37**, 931 (1980).
[4]S. T. Picraux, L. R. Dawson, G. C. Osbourn, R. M. Biefeld, and W. K. Chu, Appl. Phys. Lett. **43**, 1020 (1983).
[5]W. K. Chu, J. A. Ellison, S. T. Picraux, R. M. Biefeld, and G. C. Osbourn, Nucl. Instrum Methods **218**, 81 (1983).
[6]W. K. Chu, C. K. Pan, and C.-A. Chang, Phys. Rev. B **28**, 4033 (1983).
[7]J. M. Brown, N. Holonyak, Jr., M. J. Ludowise, W. T. Dietze, and C. R. Lewis, Appl. Phys. Lett. **43**, 863 (1983).
[8]W. J. Bartels and W. Nijman, J. Cryst. Growth **44**, 518 (1978).
[9]W. J. Bartels and H. Veenliet, Inst. Phys. Conf. Ser. (1979) No. 45, Chap. 3, p. 229.
[10]V. S. Speriosu and H. L. Glass, U.S./France Seminar on Topography, Snowmass, Colorado, 1983.
[11]V. S. Speriosu, M-A. Nicolet, J. L. Tandon, and Y. C. M. Yeh (unpublished).
[12]J. Burgeat and D. Taupin, Acta Crystallogr. **A24**, 99 (1968).
[13]A. Fukuhara and Y. Takano, Acta Crystallogr. **A33**, 137 (1977).
[14]B. C. Larson and J. F. Barhorst, J. Appl. Phys. **51**, 3181 (1980).
[15]K. Komenou, I. Hirai, K. Asama, and M. Sakai, J. Appl. Phys. **49**, 5816 (1978).
[16]V. S. Speriosu, J. Appl. Phys. **52**, 6094 (1981).
[17]V. S. Speriosu, B. M. Paine, M-A. Nicolet, and H. L. Glass, Appl. Phys. Lett. **40**, 604 (1982).
[18]B. M. Paine, V. S. Speriosu, L. S. Wielunski, H. L. Glass, and M-A. Nicolet, Nucl. Instrum. Methods **191**, 80 (1981).
[19]V. S. Speriosu and C. H. Wilts, J. Appl. Phys. **54**, 3325 (1983).
[20]Armin Segmüller, P. Krishna, and L. Esaki, J. Appl. Cryst. **10**, 1 (1977).
[21]R. M. Fleming, D. B. McWhan, A. C. Gossard, W. Wiegmann, and R. A. Logan, J. Appl. Phys. **51**, 357 (1980).
[22]J. Hornstra and W. J. Bartels, J. Cryst. Growth **44**, 513 (1978).
[23]W. H. Zachariasen, *Theory of X-Ray Diffraction in Crystals* (Wiley, New York, 1945).
[24]Speriosu is grateful to Drs. Lehel Zsoldos and Armin Segmüller for questioning the general validity of Eq. (6) in Ref. 16.
[25]V. S. Speriosu, M-A. Nicolet, S. T. Picraux, and R. M. Biefeld, Appl. Phys. Lett. **45**, 223 (1984).
[26]We thank Y. C. M. Yeh and J. L. Tandon of Applied Solar Energy Corporation for providing GaAlAs/GaAs superlattices.
[27]We thank W. K. Chu of the University of North Carolina at Chapel Hill for providing AlSb/GaSb superlattices.
[28]J. A. Ibers and W. C. Hamilton, eds., *International Tables for X-Ray Crystallography*, Vol. IV (Kynoch, Birmingham, 1974).
[29]G. A. Rozgonyi, P. M. Petroff, and M. B. Panish, J. Cryst. Growth **27**, 106 (1974).
[30]E. Estop, A. Izrael, and M. Sauvage, Acta Crystallogr. **A32**, 627 (1976).
[31]See, for example, R. F. S. Hearmon, *An Introduction to Applied Anisotropic Elasticity* (Oxford University, New York, 1961).
[32]M. K. Farr, J. G. Taylor, and S. K. Sinha, Phys. Rev. B **11**, 1587 (1975).